Collision Avoidance Method of Humanoid Robot with Arm Force

Eijiro Ohashi, Takahiro Aiko, Toshiaki Tsuji, and Kouhei Ohnishi
Keio University
Department of System Design Engineering
3-14-1, Hiyoshi, Kohoku, Yokohama, Japan
(ei2ro, aiko, tsuji, ohnishi)@sum.sd.keio.ac.jp

Abstract— **This paper describes a collision avoidance method of the biped robot with the upper body. We propose the method that the robot stops in front of an obstacle by generating arm force. When the robot detects the obstacle by the arm tip, it should stop short of the obstacle in order to avoid crush. Hence, in this paper, we propose the method of trajectory planning with the arm force. The arm force is generated as a function of the distance from the robot body to the obstacle. The closer the robot approaches to the obstacle, the larger the arm force becomes. When the obstacle is unmovable, the robot can stop with exerting arm force. If it is movable, the robot continues walking with pushing motion. Linear inverted pendulum mode (LIPM) and orbital energy are introduced. We add the dynamics of the arm force to LIPM and orbital energy. The index of orbital energy implies the limit to recognize whether the robot can stop or not at the moment of contact.**

Key Words: **biped robot, humanoid robot, walking robot, pushing motion, arm force, manipulation**

1 Introduction

In recent years, legged robots have been developed and become able to walk just like human beings. They are superior to robots with wheels or crawlers, in traveling around human environment which has holes, steps, and bumps.

A lot of researches about biped robots have focused on walking motion itself. Although walking motion has been investigated for about 30 years, cooperative motion between the upper body and the lower body has been discussed only for the last decade. Harada *et al.* studied ZMP (zero moment point) analysis of the humanoid robot under pushing motion[1][2][3]. They proposed GZMP (generalized ZMP) which takes account of the dynamics of the pushing arm. The fundamental ZMP trajectory is based on the trajectory with no contact force. When the robot pushes the object, the ZMP trajectory is modified by a certain amount. Hwang *et al.* studied the static stability about motion of pushing a wall and motion of twisting a valve while the humanoid robot does not step[4]. Yoshida *et al.* investigated the humanoid robot which has tasks with its arms[5][6]. When the external force is small or the arm tip moves in narrow space, the robot keeps double support phase. On the other hand, when the large force affects the robot or the arm tip has to move in wide range, the robot makes a step and recovers its stability.

In this paper, we consider pushing motion with upper body of humanoid robot. There are few researches which uses the arm force to stop when the robot reaches unknown environments, such that walls, doors, human beings, etc. We define these environment as "obstacle", and discuss the contact motion to the obstacle. If the arm tip detects the obstacle, the robot must stop in front of it. However, by only modifying the walking trajectory, ankle torque must suppress enormous energy of walking. If the robot cannot generate enough ankle torque, it may crush to the obstacle. Even if the ankle torque can be generated sufficiently, it may cause walking unstableness. In either case, the robot cannot continue to be in a stable condition.

In this research, the robot pushes the obstacle with the arm in order not to crush against the obstacle. Under this motion, the arm force should be variable. When the robot touches unknown obstacle, the robot must adapt to it. In other words, in order to be compliant to the obstacle, the arm force should be zero at a moment of contact. Thereafter, the arm force increases gradually to decelerate the robot body and to detect whether the obstacle is movable or not. Hence, the arm force is modified corresponding to the distance from the obstacle. It is appropriate for contact motion that the closer the robot approaches to the obstacle, the larger the arm force should become. If the robot exerts the sudden large arm force to the obstacle, it may move far away from the robot or it may be broken.

We introduce the index of orbital energy[7] proposed by Kajita *et al.*. In this paper, linear inverted pendulum mode (LIPM) is applied to generate the walking trajectory. We develop this index by adding the term of arm force. With the extended index, it can be predicted whether the robot can stop short of the obstacle at an arbitrary condition. When it is expected that the robot cannot stop, larger force should be generated from the beginning.

0-7803-8662-0/04/$20.00 ©2004 IEEE

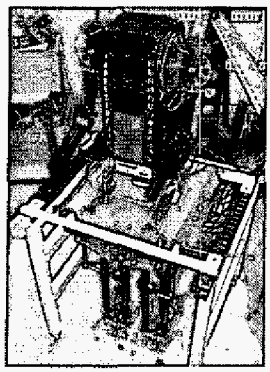

Fig. 1: Overview of the Humanoid Robot

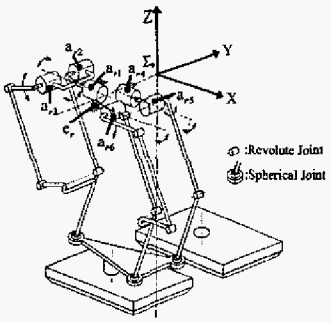

Fig. 2: Structure of the Leg

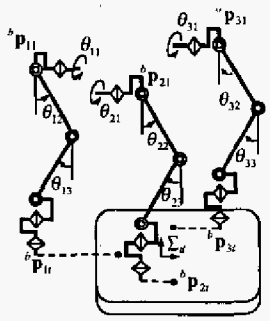

Fig. 3: Left Leg Model

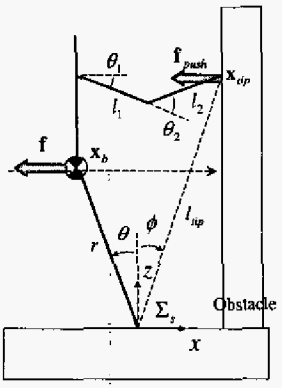

Fig. 4: Kinematic Relationship

We assume that contact between the obstacle and the arm tip is stable. The robot has no external sensors to detect an obstacle beforehand. The upper body and the lower body are coupled mechanically. We consider the motion of the robot in sagittal plane.

With the proposed method, when the arm tip touches an unknown obstacle, the robot can stop short of it with the arm force. Even if the obstacle is a movable object, the robot can continue walking motion. Consequently, the robot adapts to an unknown environment, and modifies the walking trajectory appropriately.

Contents of this paper are as follows: In section 2, the model of the humanoid robot which has an upper body with the arm is shown. In section 3, LIPM and its orbital energy are explained. In section 4, we propose a collision avoidance method with pushing motion of the arms. The method makes the robot compliant to an unknown obstacle. Experimental results are shown in section 5. Finally, this paper is concluded in section 6.

2 Modeling

Fig. 1 shows the overview of the humanoid robot. The model of the leg is shown in Fig. 2. The base coordinate system, Σ_b, is defined as the center of the located joint plane. Hereinafter, we will represent only kinematics of the left leg and the left arm. Those of the right leg and the right arm can be also expressed as the same way. The kinematic relationship from the base to the foot tip is denoted as follows:

$$ {}^b\boldsymbol{x}_{foot} = \begin{bmatrix} {}^b\boldsymbol{p}_{foot} \\ {}^b\boldsymbol{a}_{foot} \end{bmatrix}. \tag{1} $$

where ${}^b\boldsymbol{p}_{foot}$ is the position vector of each foot in Σ_b, and ${}^b\boldsymbol{a}_{foot}$ is the direction vector which expresses the posture of the foot in Σ_b. Inverse kinematics can be obtained as follows:

$$ \boldsymbol{\theta}_{leg} = \boldsymbol{F}({}^b\boldsymbol{x}_{foot}) \tag{2} $$

where $\boldsymbol{\theta}_{leg} = [\theta_{11}, \theta_{12}, \theta_{13}, \theta_{21}, \theta_{21}, \theta_{33}]^T$ is an active joint angle vector as shown in Fig. 3. $\boldsymbol{F}(\cdot)$ is the function of kinematics from the foot position to joint angles. Jacobian matrix of parallel mechanism, $\boldsymbol{J}_{leg}$, is defined as follows unlike serial mechanism:

$$ \dot{\boldsymbol{\theta}}_{leg} = \frac{\partial \boldsymbol{F}({}^b\boldsymbol{x}_{foot})}{\partial\, {}^b\boldsymbol{x}_{foot}}\, {}^b\dot{\boldsymbol{x}}_{foot} \tag{3} $$

$$ = \boldsymbol{J}_{leg}({}^b\boldsymbol{x}_{foot})\, {}^b\dot{\boldsymbol{x}}_{foot}. \tag{4} $$

Details of kinematics and dynamics of the leg are described in reference [8].

The model of the upper body in sagittal plane is shown in Fig. 4. Kinematic relationship from the base to the arm tip is represented as follows:

$$ {}^b\boldsymbol{x}_{tip} = \begin{bmatrix} l_1 C_1 + l_2 C_{12} + {}^b x_{sh} \\ -l_1 S_1 - l_2 S_{12} + {}^b z_{sh} \end{bmatrix}. \tag{5} $$

${}^b\boldsymbol{x}_{tip} = [{}^b x_{tip}, {}^b z_{tip}]^T$	: arm tip position in Σ_b
${}^b\boldsymbol{x}_{sh} = [{}^b x_{sh}, {}^b z_{sh}]^T$	: shoulder joint position in Σ_b
$\boldsymbol{\theta}_{arm} = [\theta_1, \theta_2]^T$	: arm joint angle
l_i	: length of arm link i
S_i, C_i	: $\sin\theta_i$, $\cos\theta_i$
S_{ij}, C_{ij}	: $\sin(\theta_i + \theta_j)$, $\cos(\theta_i + \theta_j)$

Jacobian matrix of the arm, $\boldsymbol{J}_{arm}$, is defined as follows:

$$ {}^b\dot{\boldsymbol{x}}_{tip} = \boldsymbol{J}_{arm}\dot{\boldsymbol{\theta}}_{arm}. \tag{6} $$

$$ \boldsymbol{J}_{arm} = \begin{bmatrix} -l_1 S_1 - l_2 S_{12} & -l_2 S_{12} \\ -l_1 C_1 - l_2 C_{12} & -l_2 C_{12} \end{bmatrix} $$

Table 1: Parameters of the Robot

		Size[mm]	Mass[kg]
Upper Body	Body	$173 \times 200 \times 560$	6.0
	Upper Arm	200	0.7×2
	Lower Arm	230	0.3×2
Lower Body	Body	$519 \times 472 \times 132$	19.4
	Thigh	300	1.5×2
	Shin	300	0.5×2
	Foot	$142 \times 270 \times 55$	2.1×2

Manipulating force is represented as follows:

$$\boldsymbol{\tau} = \boldsymbol{J}_{arm}^T \boldsymbol{f}_{push} \quad (7)$$

$$\begin{bmatrix} \tau_1 \\ \tau_2 \end{bmatrix} = \begin{bmatrix} -l_1 S_1 - l_2 S_{12} \\ -l_2 S_{12} \end{bmatrix} f_{push,x} \quad (8)$$

$$= \begin{bmatrix} {}^b z_{tip} - {}^b z_{sh} \\ -l_2 S_{12} \end{bmatrix} f_{push,x} \quad (9)$$

where $\boldsymbol{\tau} = [\tau_1, \tau_2]^T$ is the joint torque vector of the arm, and $\boldsymbol{f}_{push} = [f_{push,x}, 0]^T$ is the horizontal arm force exerted at the arm tip to the obstacle. We assume that the arm force has only the horizontal component. Considering the torque limits of the arm joints, the maximum arm force varies corresponding to the arm tip position from the shoulder. From (9) and torque limit of each arm joint, the maximum arm force, $\boldsymbol{f}_{max}$ is determined.

Since the robot has small mass of the leg and the arm as shown in Table 1, dynamics of the swing leg and the arm is negligible and the COG (center of gravity) position of the robot scarcely varies. It is more appropriate than serial link robots that the robots approximate the inverted pendulum.

3 LIPM and Orbital Energy

Linear inverted pendulum mode (LIPM) and orbital energy[7] were proposed by Kajita *et al.*. In this section, LIPM and its orbital energy are introduced. When the COG height of the robot is constant, LIPM is represented as the following equation.

$$\ddot{x}_b = \frac{g}{z_b} x_b \quad (10)$$

The robot needs no ankle torque as long as the robot tracks the trajectory of LIPM. An analytical solution of (10) is as follows:

$$x_b(t) = x_0 \cosh(\omega t) + \frac{\dot{x}_0}{\omega} \sinh(\omega t) \quad (11)$$

$$\dot{x}_b(t) = \left\{ x_0 \sinh(\omega t) + \frac{\dot{x}_0}{\omega} \cosh(\omega t) \right\} \omega \quad (12)$$

where $\omega = \sqrt{g/z_b}$, $x_0 = x_b(0)$, and $\dot{x}_0 = \dot{x}_b(0)$. When LIPM is applied, orbital energy is denoted as follows:

$$E = \frac{1}{2}\dot{x}_b^2 - \frac{g}{2z_b} x_b^2 \quad (13)$$

$$= const.$$

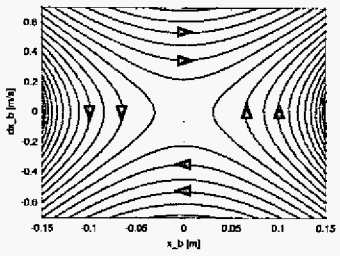

Fig. 5: Phase Plane of LIPM

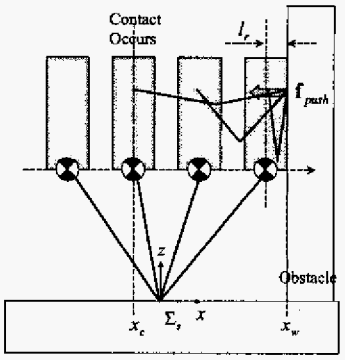

Fig. 6: Pushing Motion with LIPM

When $E > 0$, the body swings from the minus side to the plus side in x axis. $E = 0$ represents the equilibrium state. When $E < 0$, the body never goes over the supporting point. In other words, orbital energy is an index which discriminates whether the robot stops or not. Phase plane of x_b is shown in Fig. 5.

4 Proposed Method

In this section, we propose the collision avoidance method with arm force. With this method, the robot can stop in front of the obstacle with exerting the arm force. Even if the obstacle moves, the robot can continue to walk with pushing it. In addition, we extend the orbital energy[7] in order to discriminate whether the robot can stop short of the obstacle.

Hereinafter, we express each position in the supporting point coordinates system, Σ_s, as shown in Fig. 4. The origin of Σ_s is defined at the ankle joint. Each variable in Fig. 4 is represented as follows:

- $\boldsymbol{x}_b$: COG position ($= [x_b, z_b]^T$) in Σ_s
- $\boldsymbol{x}_{tip}$: arm tip position ($= [x_{tip}, z_{tip}]^T$) in Σ_s
- r : length from the ankle joint to the COG
- l_{tip} : length from the ankle joint to the arm tip
- θ : angle from the vertical to the COG
- ϕ : angle from the vertical to the arm tip

where

$$l_{tip} = \sqrt{x_{tip}^2 + z_{tip}^2} \quad (14)$$

$$z_b = r \cos\theta \quad (15)$$

$$z_{tip} = l_{tip}\cos\phi. \quad (16)$$

When the arm tip pushes the obstacle as shown in Fig. 6, f_{push} acts on the robot. For simplicity, we assume that f_{push} has only horizontal component.

In order to consider the motion of the COG, f_{push} should be transformed to the force which acts on the COG of the robot, f. Since LIPM is introduced, the following equilibrium of moment around the ankle joint is derived.

$$f\cos\theta \cdot r = f_{push}\cos\phi \cdot l_{tip} \quad (17)$$

$$\therefore\ f = \frac{z_{tip}}{z_b} \cdot f_{push} \quad (18)$$

Considering the pushing force, we extend LIPM as follows:

$$\ddot{x}_b = \frac{g}{z_b}x_b - \frac{f}{m}. \quad (19)$$

Note that the COG height is constant and that no ankle torque is needed to track this trajectory. Therefore, the walking motion is always stable since ZMP of the robot is always at the supporting point.

In an unknown environment, at the moment that the arm tip detects an obstacle, the robot should not push the obstacle but be compliant to it. Then the robot increases the arm force gradually in order to stop and to detect whether the obstacle is movable or not. If the obstacle is unmovable like a wall, the robot must stop before the obstacle with utilizing the arm force. However, if the obstacle is movable like a door or other objects, the robot pushes it and walks forward.

Hence, f_{push} should vary from zero to a certain value linearly in proportion to the distance from the obstacle. We introduce the following function of the pushing force.

$$f_{push} = k_{arm}(x - x_c) \quad (20)$$

$$k_{arm} = \frac{f_{max}}{x_w - l_r - x_c}$$

where k_{arm} represents the spring coefficients of the arm force. As shown in Fig. 6, x_c is the COG position when the robot touches the obstacle first, and l_r is the length from the robot's front surface to the COG. f_{max} is the maximum force generated by the arm which is determined by torque limit of each joint and (9).

From (18) and (20), f can be represented as follows:

$$f = k(x - x_c) \quad (21)$$

$$k = \frac{z_{tip}}{z_b}k_{arm}.$$

Substituting (21) into (19), generalized solution of (19) is derived as follows:

$$x_b(t) = \left(x_c + \frac{a_f}{\omega_f^2}\right)\cosh(\omega_f t) + \frac{\dot{x}_c}{\omega_f}\sinh(\omega_f t) - \frac{a_f}{\omega_f^2} \quad (22)$$

$$\dot{x}_b(t) = \left\{\left(x_c + \frac{a_f}{\omega_f^2}\right)\sinh(\omega_f t) + \frac{\dot{x}_c}{\omega_f}\cosh(\omega_f t)\right\}\omega_f \quad (23)$$

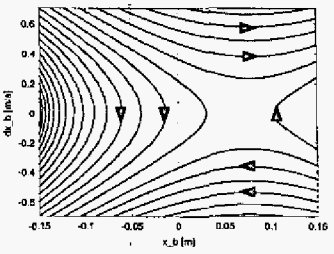

Fig. 7: Phase Plane with Pushing Force ($k = 150$)

where $\omega_f = \sqrt{\frac{g}{z_b} - \frac{k}{m}}$ and $a_f = \frac{k}{m}x_c$.

When the robot contacts the obstacle, the trajectory of the conventional LIPM, (11) and (12), is switched to trajectory described above, (22) and (23).

We extend orbital energy in consideration of the arm force. Therefore the extended orbital energy depending on (19) is derived.

$$E_f = \frac{1}{2}\dot{x}_b^2 - \frac{1}{2}\omega_f^2 x_b^2 - a_f x_b \quad (24)$$

$$= const.$$

Aspects on the phase plane are shown in Fig. 7.

To calculate $E_{f,equi}$ (E_f on equilibrium point), $\dot{x}_b = 0$ is substituted in (24).

$$E_f = -\frac{1}{2}\omega_f^2\left(x_b + \frac{a_f}{\omega_f^2}\right)^2 + \frac{a_f^2}{2\omega_f^2} \quad (25)$$

The robot is in the equilibrium state when $x_b = -a_f/\omega_f^2$ in (25). At this moment,

$$E_{f,equi} = \frac{a_f^2}{2\omega_f^2}. \quad (26)$$

When the robot is in the state which satisfies $E_f < E_{f,equi}$, the robot can stop in front of the obstacle with no step.

Although the robot exerts the arm force, it is most important where the robot steps next. The robot should stop with choosing the next step appropriately.

Hence, we derive the next step position of the swing leg. The moment of contact is defined as t_c. When the robot keeps a constant walking circle, T, the COG position and velocity of the next step are determined as $x_b(t_{rest})$ and $\dot{x}_b(t_{rest})$ in (22) and (23). Here $t_{rest} = T - t_c$. We define the parameters as Fig. 8. $l_{rest} = |x_b(t_c) - x_b(T)|$. l_{stop} determines the position of the next step.

Hereinafter, we consider based on the coordinates system of the next stop as shown in Fig. 8. The COG position during the next step is represented as $\hat{x}_b$. Here, "$\hat{}$" denotes that the parameter is in the coordinate system of the next step. The boundary condition is that $\hat{x}_0 = x_b(t_{rest})$ and $\dot{\hat{x}}_0 = \dot{x}_b(t_{rest})$. The force to the COG is represented as follows:

$$\hat{f} = k(\hat{x}_b + l_{stop} + l_{rest}) \quad (27)$$

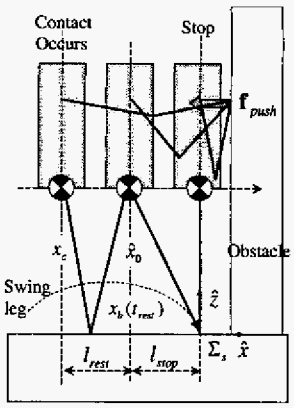

Fig. 8: The Next Step Motion

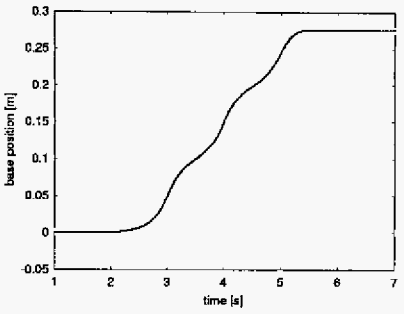

Fig. 9: Base Position

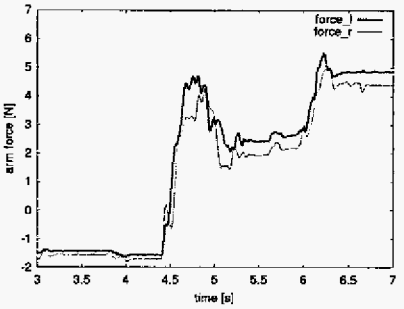

Fig. 10: f_{push} (Arm Force)

where $-l_{stop} \leq \hat{x}_b \leq 0$. On this condition, generalized solution can be derived as almost the same equations as (22) and (23). The only exception is that substitutes $\hat{a}_f = -\frac{k}{m}(l_{stop} + l_{rest})$ into a_f.

Orbital energy, $\hat{E}_f$, can be derived as the same form of (24).

$$\hat{E}_f = \frac{1}{2}\dot{\hat{x}}_b^2 - \frac{1}{2}\omega_f^2 \hat{x}_b^2 - \hat{a}_f \hat{x}_b. \tag{28}$$

Substituting $\dot{\hat{x}}_b = \dot{\hat{x}}_0$ and $\hat{x}_b = -l_{stop}$ in (28), orbital energy is derived. On the condition that the COG of the robot can stop just above the supporting point, $\hat{E}_f$ should be equal to 0. In this case, the condition of l_{stop} is derived as follows:

$$l_{stop} = \frac{\sqrt{\left(\frac{k}{m} l_{rest}\right)^2 + \dot{\hat{x}}_0^2 \left(\frac{k}{m} + \frac{g}{z_b}\right)} - \frac{k}{m} l_{rest}}{\frac{k}{m} + \frac{g}{z_b}}. \tag{29}$$

The robot can stop just above the supporting point when the robot satisfies l_{stop} of (29). This method which determines the next supporting point is applicable to the case that the robot steps 2 times or more during pushing motion.

ZMP of the robot is always at the supporting point of the LIPM. Therefore the walking motion of the robot is always stable with the proposed trajectory.

If k is too large, the COG may not go over the supporting point, i.e., the robot will go backward. It is undesirable in many situations. Therefore, in this case, the spring coefficient of the arm should become smaller. Applying the following spring coefficient after contact, the robot will stop just above the supporting point.

$$k_{stop} = m\left(\frac{\dot{x}_c^2}{x_c^2} - \frac{g}{z_b}\right) \tag{30}$$

k_{stop} is the spring coefficient which achieves $E_f = 0$ when the boundary condition is given as x_c and $\dot{x}_c$.

If the obstacle moves, the trajectory of (22) and (23) will be switched to the following trajectory which has constant force, f_v. Constant force is exerted in the case the viscous friction between the obstacle and the ground is dominant.

$$x_b(t) = \left(x_v - \frac{f_v}{m\omega^2}\right)\cosh(\omega t) + \frac{\dot{x}_v}{\omega}\sinh(\omega t) + \frac{f_v}{m\omega^2} \tag{31}$$

$$\dot{x}_b(t) = \left\{\left(x_v - \frac{f_v}{m\omega^2}\right)\sinh(\omega t) + \frac{\dot{x}_v}{\omega}\cosh(\omega t)\right\}\omega \tag{32}$$

x_v and $\dot{x}_v$ are x_b and $\dot{x}_b$ at the moment that the trajectory switches to (31) and (32). With the trajectory of (31) and (32), the region of ZMP has a margin which deals with a quantity of the force change.

5 Experiment

In the experiment, each parameter was set as follows: $f_{max} = 15$N, $l_r = 0.20$m, length of stride was 0.1m, and walking cycle was 1.0s. The aluminum board was placed in front of the robot as an obstacle. The trajectory of the swing leg was given by the polynomial which achieved the continuity of acceleration.

Results of the experiment are shown in Fig. 9, 10, 11 and 12. The robot started to walk at 2s. The robot contacted with the obstacle at around 4.55s. Then the robot switched to the proposed trajectory. The length of stride is modified into 0.077m. The robot could stop around 0.1m short of the obstacle at 6s. Orbital energy E_f was equal to 0.0015.

As shown in Fig. 9, the robot modified the trajectory smoothly in order to stop. External force was

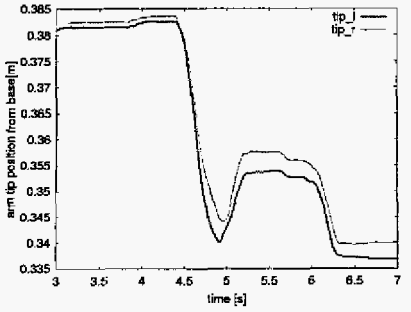

Fig. 11: Tip Position in Σ_b

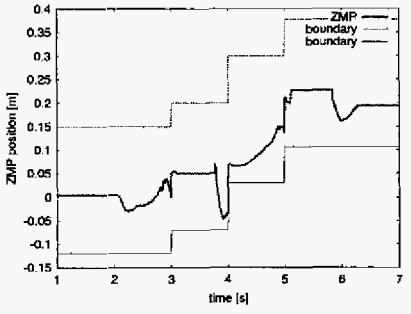

Fig. 12: ZMP of the Robot

estimated by reaction force observer[9]. From the Fig. 10 and 11, pushing motion of spring characteristic was achieved substantially although there is an offset on estimated force. The robot could stop with the constant pushing force about 5N. We consider that the aluminium board was bent mechanically from 5s to 6s. Therefore the pushing force was reduced.

ZMP of the robot is shown in Fig. 12. ZMP existed in the stable region of the plantar surface. Therefore, it indicates that the robot could keep stable walking.

From the experimental results, it is verified that the robot could stop short of the obstacle with the proposed method.

6 Conclusion

In this paper, pushing manipulation of the biped robot is discussed. We extended orbital energy for pushing motion. Extended orbital energy detects whether the robot can stop or not. Appropriate landing points can be determined by the orbital energy.

The proposed method is that the robot pushes the obstacle with compliance, then increasing the arm force. The robot can stop short of the obstacle if it is unmovable like a wall, then the robot avoids collision with the obstacle. If the obstacle moves like a door, the robot pushes it and can continue walking. With the proposed method, the robot can contact with unknown environment with the arm tip. Then the robot stops or keeps on walking with compliance to the obstacle without losing the stability.

Acknowledgement

This study was performed through Special Coordination Funds of the Ministry of Education, Culture, Sports, Science and Technology of the Japanese Government.

References

[1] K.Harada, *et al.*, "Real-Time Planning of Humanoid Robot's Gait for Force Controlled Manipulation" *in Proc. of IEEE Int. Conf. on Robotics and Automation (ICRA '04)*, Vol. 1, pp. 616–622, 2004

[2] K.Harada, *et al.*, "Pushing Manipulation by Humanoid Considering Two-Kinds of ZMPs" *in Proc. of IEEE Int. Conf. on Robotics and Automation (ICRA '03)*, Vol. 2, pp. 1627–1632, 2003

[3] K.Harada, *et al.*, "Zmp Analysis for Arm/Leg Coordination" *in Proc. of IEEE/RSJ Int. Conf. on Intelligent Robots and Systems (IROS 2003)*, Vol. 1, pp .75–81, 2003

[4] Yoonkwon Hwang, *et al.*, "Whole Body Cooperative Tasks and Static Stability Evaluations for a Humanoid Robot" *in Proc. of IEEE/RSJ Int. Conf. on Intelligent Robots and Systems (IROS 2003)*, Vol. 2, pp .1901–1906, 2003

[5] H.Yoshida, *et al.*, "Mobile Manipulation of Humanoid Robots - Analysis of Manipulability and Stability in Mobile Manipulation" *in Proc. of IEEE/RSJ Int. Conf. on Intelligent Robots and Systems (IROS 2000)*, Vol. 3, pp .1924–1929, 2000

[6] H.Yoshida, *et al.*, "Mobile Manipulation of Humanoid Robots - Method of Adjusting Leg Motion for Improvement of Arm's Manipulability" *in Proc. of IEEE/RSJ Int. Conf. on Intelligent Robots and Systems (IROS 2001)*, Vol. 1, pp .266–271, 2001

[7] S.Kajita, *et al.* "Dynamic Walking Control of a Biped Robot Along a Potential Energy Conserving Orbit" *IEEE Trans. on Robotics and Automation*, Vol. 8, No. 4, pp. 431–438, 1992

[8] M.Morisawa, *et al.* "A Walking Pattern Generation for Biped Robot with Parallel Mechanism by Considering Contact Force", *in Proc. of IEEE Int. Conf. on Industrial Electronics Society (IECON'01)*, Vol. 3, pp. 2184–2189, 2001

[9] T.Murakami, *et al.* "Torque Sensorless Control in Multidegree-of-Freedom Manipulator", *IEEE Trans. on Industrial Electronics*, Vol. 40, No. 2, pp. 259–265, 1993